Available online at www.sciencedirect.com

jmr&t
Journal of Materials Research and Technology
https://www.journals.elsevier.com/journal-of-materials-research-and-technology

Original Article

Effect of Nd-Y co-substitution on structural, magnetic, optical and microwave properties of NiCuZn nanospinel ferrites

M.A. Almessiere[a,*], Y. Slimani[a,*], A.V. Trukhanov[b,c,d], A. Demir Korkmaz[e], S. Guner[f], S. Akhtar[a], Sagar E. Shirsath[g], A. Baykal[h], I. Ercan[a]

[a] Department of Biophysics, Institute for Research and Medical Consultations (IRMC), Imam Abdulrahman Bin Faisal University, P.O. Box 1982, 31441 Dammam, Saudi Arabia
[b] SSPA "Scientific and Practical Materials Research Centre of NAS of Belarus", 19, P. Brovki Str., 220072 Minsk, Belarus
[c] South Ural State University, 76, Lenina Ave., 454080, Chelyabinsk, Russia
[d] National University of Science and Technology MISiS, Moscow, 4, Leninsky Prospekt 119049, Russia
[e] Department of Chemistry, Istanbul Medeniyet University, 34700 Uskudar-Istanbul, Turkey
[f] Institute of Inorganic Chemistry, RWTH Aachen University, D-52074 Aachen, Germany
[g] School of Materials Science and Engineering, University of New South Wales, Kensington, Sydney, NSW 2052, Australia
[h] Department of Nanomedicine Research, Institute for Research and Medical Consultations (IRMC), Imam Abdulrahman Bin Faisal University, P.O. Box 1982, 31441 Dammam, Saudi Arabia

ARTICLE INFO

Article history:
Received 13 May 2020
Accepted 6 August 2020
Available online 20 August 2020

Keywords:
Spinel ferrites
Optical properties
Magnetization
Microwave properties

ABSTRACT

Partially Nd/Y substituted $[Ni_{0.4}Cu_{0.2}Zn_{0.4}](Nd_xY_xFe_{2-2x})O_4$ ($x \leq 0.05$) spinel ferrite nanoparticles (NSFs) were prepared by citrate sol-gel auto-combustion technique. UV–vis Percent to determine optoelectronic properties mixed spinel ferrite materials. Direct energy band gaps values are within 1.87 and 1.92 eV interval. The magnetization features were investigated at room temperature (RT; T = 300 K) versus magnetic field ((*M-H*)). RT M-H curves showed superparamagnetic (SPM) behavior in non-substituted sample (x = 0.00), while all the Nd-Y substituted NiCuZn ferrite NPs exhibited soft ferrimagnetic (FM) character. It is found that the magnitude of magnetization drops with a rise in Nd^{3+} and Y^{3+} contents. ZFC–FC magnetization curves revealed the existence of dipolar interactions, which illuminate a partially blocked state in accordance with M-H loops at 300 K. The electrodynamic data reflection coefficients for $Ni_{0.4}Cu_{0.2}Zn_{0.4}](Nd_xY_xFe_{2-2x})O_4$ ($x \leq 0.05$) NSFs were determined. The occurrences of the electromagnetic absorption between 49 to 4.15 GHz frequency range were observed. A significant linking amongst the ratio (x) and amplitude-frequency characteristics (AFC) was investigated. Additionally, the AFC of the $Ni_{0.4}Cu_{0.2}Zn_{0.4}](Nd_xY_xFe_{2-2x})O_4$ ($x \leq 0.05$) NSFs were strongly influenced with the increase of Nd/Y concentration. It was demonstrated that low level of the concentration substitution (less than 10 at.%) not critically effected on resonance characteristics. We found that an anomalous altering of the

* Corresponding authors.
E-mails: malmessiere@iau.edu.sa (M. Almessiere), yaslimani@iau.edu.sa (Y. Slimani).
https://doi.org/10.1016/j.jmrt.2020.08.027

resonant amplitude (almost 2 times) resulted due the manifestation of indirect exchange interactions amongst iron (III), yttrium (III) and neodymium (III) electronic shells. Almost a linear behavior of the main AFC was observed.

1. Introduction

Spinel ferrite nanoparticles (FNPs) are a class of magnetic materials within the nanometer region in either direction in their structure. They are being used in biomedicine including magnetic hyperthermia, biosensors, magnetic resonance imaging (MRI), immunoassays, tissue engineering and drug delivery; electronics including information storage systems, rechargeable lithium batteries, data storage, and magnetic bulk cores, environmental applications such as gas sensors and catalysts and military uses as microwave absorbers [1–8]. NiCuZn ferrites are soft magnetic materials that can act as high-frequency components with their characteristics such as low eddy current losses, high resistivity, high permeability along with low-cost of production and especially used to reduce radar signatures and for the elimination of electromagnetic interference (EMI) [9]. To achieve these goals, recent demands require materials that can work in the 1−20 GHz frequency range [10]. For that reason, materials with novel properties should be developed.

The properties of FNPs can be tuned by varying the cation components in their structure with other divalent or trivalent ions. Therefore, we can produce microwave absorbing NiCuZn FNPs either by changing the amount of nickel, copper, zinc and/or iron ions in the formula or by substituting with different cations. Researchers worldwide have studied microwave-absorption characteristics of NiCuZn FNPs. For example, J.C. Aphesteguy et al. [10] applied the citrate-assisted auto-combustion method to prepare NiCuZn FNPs ($Ni_{0.35}Cu_{0.15}Zn_{0.5}Fe_2O_4$) as well as NiZn FNPs, which were then coated with epoxy resin for microwave measurements. The results indicated that $Ni_{0.35}Cu_{0.15}Zn_{0.5}Fe_2O_4$ FNPs displayed a wide range of microwave absorption between 1 MHz and 1.8 GHz. The substitution of copper also elevated the tan δ (dielectric losses) at 1.3 GHz to <0.01 compared to only 0.006 in NiZn FNPs [10]. Akhtar and co-workers fabricated a nanocomposite of $Ni_{0.6}Cu_{0.2}Zn_{0.2}Fe_2O_4$/PVDF and MWCNT by a sol-gel combustion technique. The nanocomposites were sintered at different temperatures (size range 26−34 nm) and were evaluated for their electromagnetic characteristics [11]. The dielectric constant (ε') and imaginary part of the dielectric constant (ε'') both enhanced at lower frequencies while an opposite behavior was seen at higher frequencies, which is a typical behavior in ferrite materials. The authors added that the polarization can also affect this dielectric constant which can be attributed to the space charge polarization with respect to the applied magnetic field. Their results showed initial permeability was enhanced and the relative loss decreased with sintering temperature and addition of MWCNT, which shows the nanocomposite could be used for high-frequency and electromagnetic applications. Hashim et al. substituted the trivalent iron ion in NiCuZn to obtain $Ni_{0.5}Cu_{0.25}Zn_{0.25}Fe_{2-x}In_xO_4$ FNPs ($x = 0.0$, 0.1, 0.2, 0.3 and 0.4) by a citrate-gel method (size range 25–34 nm). As the iridium component increased, Curie temperature dropped from 698 K to 653 K. The blocking temperature was found to be 325 K by FC and ZFC magnetization measurements. Above the blocking temperature, the materials showed superparamagnetic behavior indicating they could be used for biomedical applications. Recently, our group synthesized Tb^{3+} substituted NiCuZn FNPs by an ultrasonic method. Magnetic measurements revealed the superparamagnetic trait of FNPs at 300 K and soft ferromagnetic behavior at low temperature (10 K) [12]. We also applied the sonochemical assisted technique to prepare $Ni_{0.3}Cu_{0.3}Zn_{0.4}Tm_xFe_{2-x}O_4$ ($0.0 \le x \le 0.10$) FNPs. The magnetic measurements proved that Tm^{3+} substituted NiCuZn FNPs had a similar behavior to those found in Tb^{3+} substituted counterparts. On the other hand, H_c, M_r, M_s, and n_B values dropped as the amount of Tm^{3+} substitution increases. Furthermore, numerous researchers have studied the effect of Nd^{3+} or Y^{3+} ions on the magnetic and microwave properties of spinel ferrites. Pranav P. Naik and his group produced manganese zinc ferrite doped with neodymium (Nd^{3+}) with chemical formula $Mn_{0.6}Zn_{0.4}Nd_xFe_{2-x}O_4$ ($x = 0.04$, 0.05, 0.06, 0.07 and 0.08) nanoparticles by combustion method [13]. They found that saturation magnetization can be tuned in a systematic manner by changing the concentration of Nd^{3+} ions. Moreover, Kun Qian et al. [14] synthesized variant ratios of $Ni_{0.5}Zn_{0.5}Nd_xFe_{2-x}O_4$ through sol-gel route combined with self-propagating combustion (SPC) technique. The obtained results revealed that Nd^{3+} ions could significantly improve the dielectric properties and microwave absorption capacity at low frequencies. Silvia E. Jacobo et al. [15] studied the properties of $Ni_{0.5}Zn_{0.5}Y_yFe_{2-y}O_4$ ($0.01 \le y \le 0.05$) prepared with sol–gel method. They observed that Y substituting Ni-Zn ferrite plays an important role in the enhancement of the magnetic properties. These products can be considered as attenuator materials in the explored microwave range. Likewise, Chakrabarty et al. [16] investigated the influence of yttrium substitution on magnetic and electrical properties of cobalt ferrite. The saturation magnetization and anisotropy constant reduce as the doping element rises. In addition, the maximum electrical conductivity was observed in the 15 mol% doped sample. Accordingly, in this paper we reported Nd-Y co-substituted NiCuZn NSFs. The $[Ni_{0.4}Cu_{0.2}Zn_{0.4}](Nd_xY_xFe_{2-2x})O_4$ ($x \le 0.05$) NSFs were prepared via sol-gel auto-combustion (SGAC) approach and the various structural, microwave absorption, optical and magnetic properties of the synthesized nanoparticles were evaluated and discussed deeply.

2. Experimental

We applied the citrate sol-gel auto-combustion technique to produce NSFs with a formula of

$[Ni_{0.4}Cu_{0.2}Zn_{0.4}](Nd_xY_xFe_{2-2x})O_4$ ($x \le 0.05$). Precursor chemicals are hydrates of $Ni(NO_3)_2$, $Zn(NO_3)_2$, $Cu(NO_3)_2$, $Fe(NO_3)_3$, $Nd(NO_3)_3$, $Y(NO_3)_3$ and $C_6H_8O_7$ which were purchased from Sigma-Aldrich. Stochiometric amounts of metals nitrites and citric acid were dissolved in 100 mL of deoinized water by stirring at 90 °C for 40 min. At that point, the pH of the resultant solution was arranged at 7 using ammonia solution. The temperature was raised up to 370 °C till the solution was transformed into a gel and then burned to form black powder of $[Ni_{0.4}Cu_{0.2}Zn_{0.4}](Nd_xY_xFe_{2-2x})O_4$ ($x \le 0.05$) NSFs.

Rigaku Benchtop Miniflex XRD (with copper Kα radiation) was applied for the structural investigation. Morphological evaluation of the compositions was recorded by a scanning electron microscope (SEM; FEI Titan ST) coupled with EDX system and a transmission electron microscope (TEM; FEI, Morgagni 268). UV–vis diffuse reflectance spectra were measured between 200–800 nm. All VSM measurements were done over an applied field of H = ±70 kOe at room temperature (RT; 300 K). In addition, magnetic measurements in zero-field-cooling (ZFC) and field-cooling (FC) modes were performed as a function of temperature ranging from RT down to lower temperatures of about 2 K. These magnetic measurements were carried out using Physical Property Measurement System coupled with vibrating sample magnetometer head (PPMS-VSM Dyna Cool 9 from Quantum Design).

Agilent network analyzer has been utilized to measure the frequency dependences of S-parameters between 2 GHz and 12 GHz frequencies and the Nicholson–Ross–Weer method (NRW) was used for the calculations. The following MW reflection loss data was computed using:

$$\dot{R} = \frac{\sqrt{\frac{\mu}{\varepsilon}} - 1}{\sqrt{\frac{\mu}{\varepsilon}} + 1} \text{ or } \left|\dot{R}\right| = 10lg\left(\frac{\sqrt{\frac{\mu}{\varepsilon}} - 1}{\sqrt{\frac{\mu}{\varepsilon}} + 1}\right) \text{ in dB} \quad (1)$$

Where $\left|\dot{R}\right|$ (in dB) is the reflection coefficient modulus (the ratio of the reflected to incident wave amplitude).

3. Results and discussion

3.1. Phase analysis and morphology

Fig. 1 displayed the structural properties of $Ni_{0.4}Cu_{0.2}Zn_{0.4}](Nd_xY_xFe_{2-2x})O_4$ ($x \le 0.05$) NSFs. Miller indices of entire compositions indicated the single phase of Ni-Cu-Zn spinel phase according to ICDD card number 10-0325. No undesired secondary phases were observed. Moreover, the position of the most intense peak (311) remained the same with doping by Nd-Y indicated that the crystal was retained the cubic shape of $[Ni_{0.4}Cu_{0.2}Zn_{0.4}](Nd_xY_xFe_{2-2x})O_4$ ($x \le 0.05$) NSFs. The structural parameters and the average crystallites size were gotten through Rietveld refinement with FullProof software as seen in Table 1. It was found that the cell parameters (a) increases with the increase in the ratio of substitutions because of the differences in ionic radii of ions [17]. Scherer's equation was applied to determine the average crystallites size (D_{XRD}) of $[Ni_{0.4}Cu_{0.2}Zn_{0.4}](Nd_xY_xFe_{2-2x})O_4$ ($x \le 0.05$) NSFs. The values of D_{XRD} are between 9–15 nm. Cation distributions of the prepared sample of $[Ni_{0.4}Cu_{0.2}Zn_{0.4}](Nd_xY_xFe_{2-2x})O_4$ ($x \le 0.05$) NSFs series have been estimated by X-ray diffraction pattern based on Bertuat method [18,19] and parameters such as R_B and χ2 were calculated. The distribution of trivalent and divalent cations amongst A (tetrahedral) and B (octahedral) crystallographic sites was obtained from ratios of the intensity of I_{220}/I_{440} and I_{422}/I_{400} planes which are expected to be sensitive for cation distribution [19]. It has been observed Table 2 that Fe^{3+} ions occupied each octahedral and tetrahedral site. Havier rare-earth Nd^{3+} cation occupy

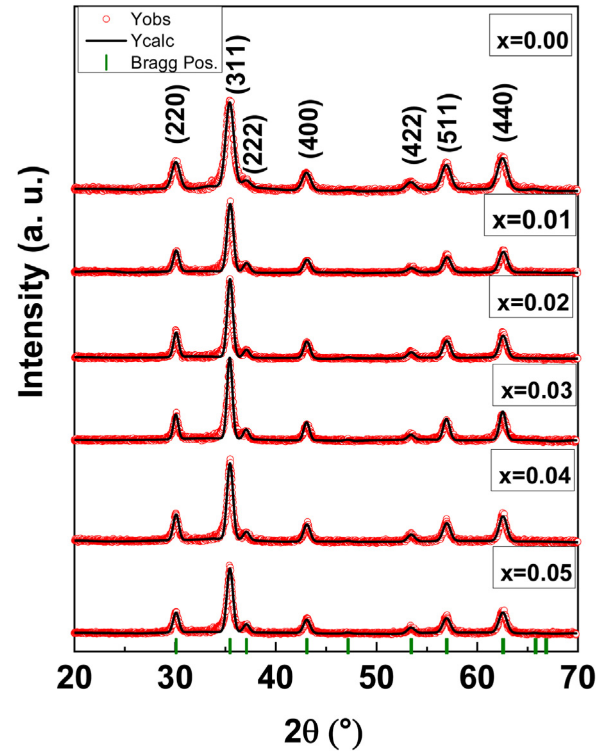

Fig. 1 – XRD powder patterns of $[Ni_{0.4}Cu_{0.2}Zn_{0.4}](Nd_xY_xFe_{2-2x})O_4$ ($0.0 \le x \le 0.05$) NSFs.

Table 1 – Nd-Y content, refined structural parameters for $Ni_{0.4}Cu_{0.2}Zn_{0.4}](Nd_xY_xFe_{2-2x})O_4$ ($0.0 < x < 0.05$) NSFs Fd-3 m (No. 227).

x	a (Å)	V (Å)³	D_{XRD} (nm) ±0.06	χ^2 (chi²)	R_{Bragg}
0.00	8.396(0)	591.86	9.51	1.36	2.73
0.01	8.406(0)	593.97	14.42	1.59	4.16
0.02	8.414(7)	595.82	14.97	1.22	3.16
0.03	8.416(2)	596.14	14.73	1.68	4.27
0.04	8.418(0)	596.52	14.20	1.26	1.83
0.05	8.422(9)	595.43	14.35	1.41	3.63

Table 2 – Cation distribution of $Ni_{0.4}Cu_{0.2}Zn_{0.4}](Nd_xY_xFe_{2-2x})O_4$ ($0.0 < x < 0.05$) NSFs.

x	Tetrahedral A-site	Octahedral B-site
0.00	$Zn_{0.4}Fe_{0.6}$	$Ni_{0.4}Cu_{0.2}Fe_{1.4}$
0.01	$Zn_{0.4}Y_{0.01}Fe_{0.59}$	$Ni_{0.4}Cu_{0.2}Nd_{0.01}Fe_{1.39}$
0.02	$Zn_{0.4}Y_{0.02}Fe_{0.58}$	$Ni_{0.4}Cu_{0.2}Nd_{0.02}Fe_{1.38}$
0.03	$Zn_{0.4}Y_{0.03}Fe_{0.53}$	$Ni_{0.4}Cu_{0.2}Nd_{0.03}Fe_{1.37}$
0.04	$Zn_{0.4}Y_{0.04}Fe_{0.56}$	$Ni_{0.4}Cu_{0.2}Nd_{0.04}Fe_{1.36}$
0.05	$Zn_{0.4}Y_{0.05}Fe_{0.55}$	$Ni_{0.4}Cu_{0.2}Nd_{0.05}Fe_{1.35}$

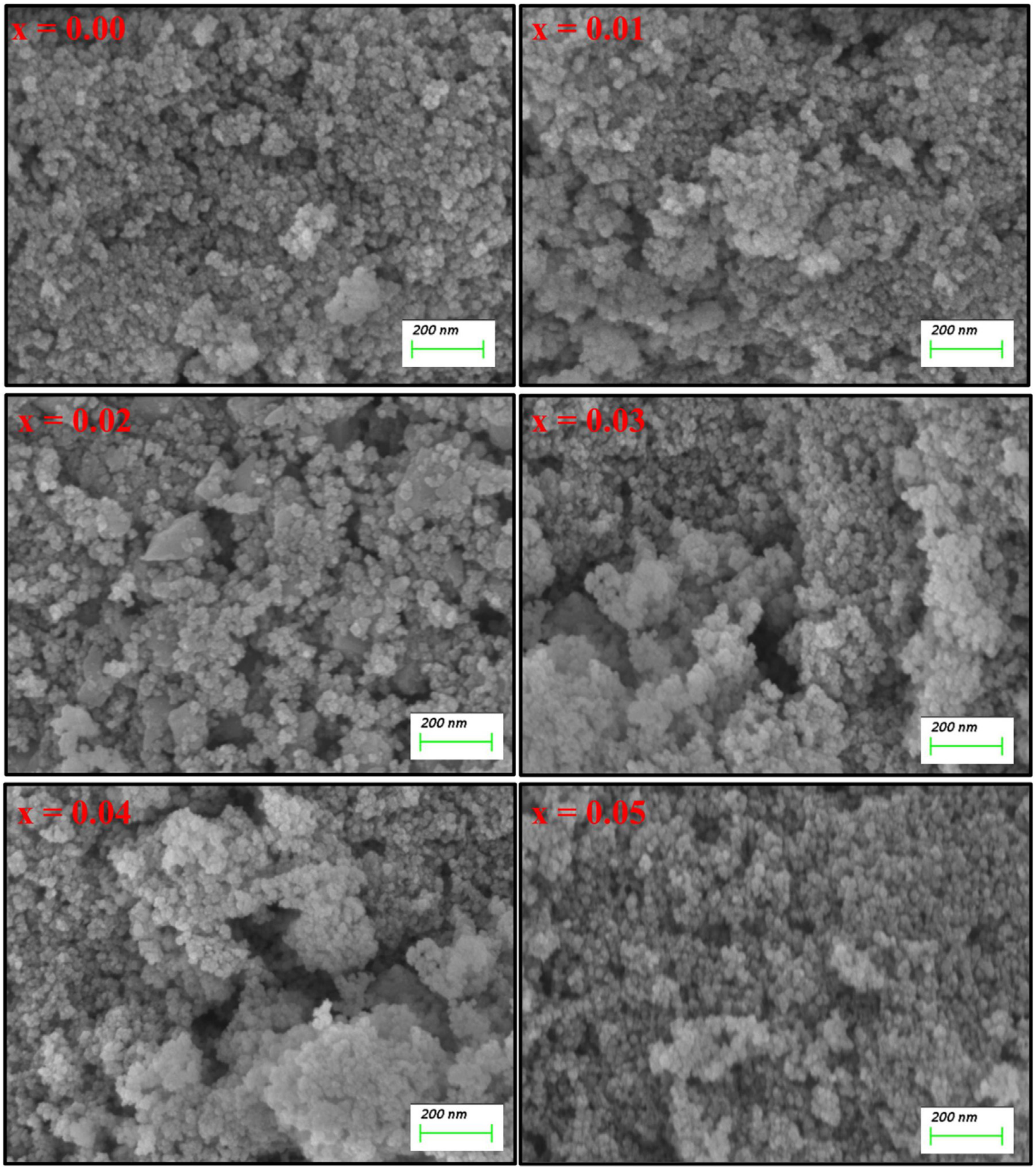

Fig. 2 – SEM images of $[Ni_{0.4}Cu_{0.2}Zn_{0.4}](Nd_xY_xFe_{2\text{-}2x})O_4$ ($0.0 \le x \le 0.05$) NSFs.

octahedral B-site due to their larger ionic radii. Y^{3+} ions accommodated into tetrahedral A-site. As expected, divalent Zn^{2+} distributed over tetrahedral A-site. Cu^{2+} and Ni^{2+} cations occupy octahedral B-site [20].

SEM micrographs of $[Ni_{0.4}Cu_{0.2}Zn_{0.4}](Nd_xY_xFe_{2\text{-}2x})O_4$ ($x \le 0.05$) NSFs were presented in Fig. 2. The grains of synthesized samples have been agglomerated and possess a spherical structure with average grains size around 20 nm which nearly to the XRD results. The quantitative investigation of $[Ni_{0.4}Cu_{0.2}Zn_{0.4}](Nd_xY_xFe_{2\text{-}2x})O_4$ ($0.01 \le 0.05$) NSFs were displayed in Fig. 3. EDX analysis are well consents with the chemical formula of the products. TEM images of $[Ni_{0.4}Cu_{0.2}Zn_{0.4}](Nd_xY_xFe_{2\text{-}2x})O_4$ ($x = 0.02$ and 0.05) NSFs are shown in Fig. 4. The particles exhibited cubic shape and aggregation attributable to their magnetic characteristics. The histograms of particles size distributions showed that the average diameter of the particles is between 10 and 20 nm, which agreed with XRD results (see Table 1). SAED pattern rings shown in Fig. 4 are labeled as (220), (311), (400), (511) and (440) (in line with XRD patterns).

3.2. *Optical properties*

Optical properties of $[Ni_{0.4}Cu_{0.2}Zn_{0.4}](Nd_xY_xFe_{2\text{-}2x})O_4$ ($x \le 0.05$) NSFs were studied applying Percent Diffuse Reflectance (DR %) measurements via UV–vis spectrophotometer. Fig. 5 indi-

J MATER RES TECHNOL. 2020;9(5):11278–11290

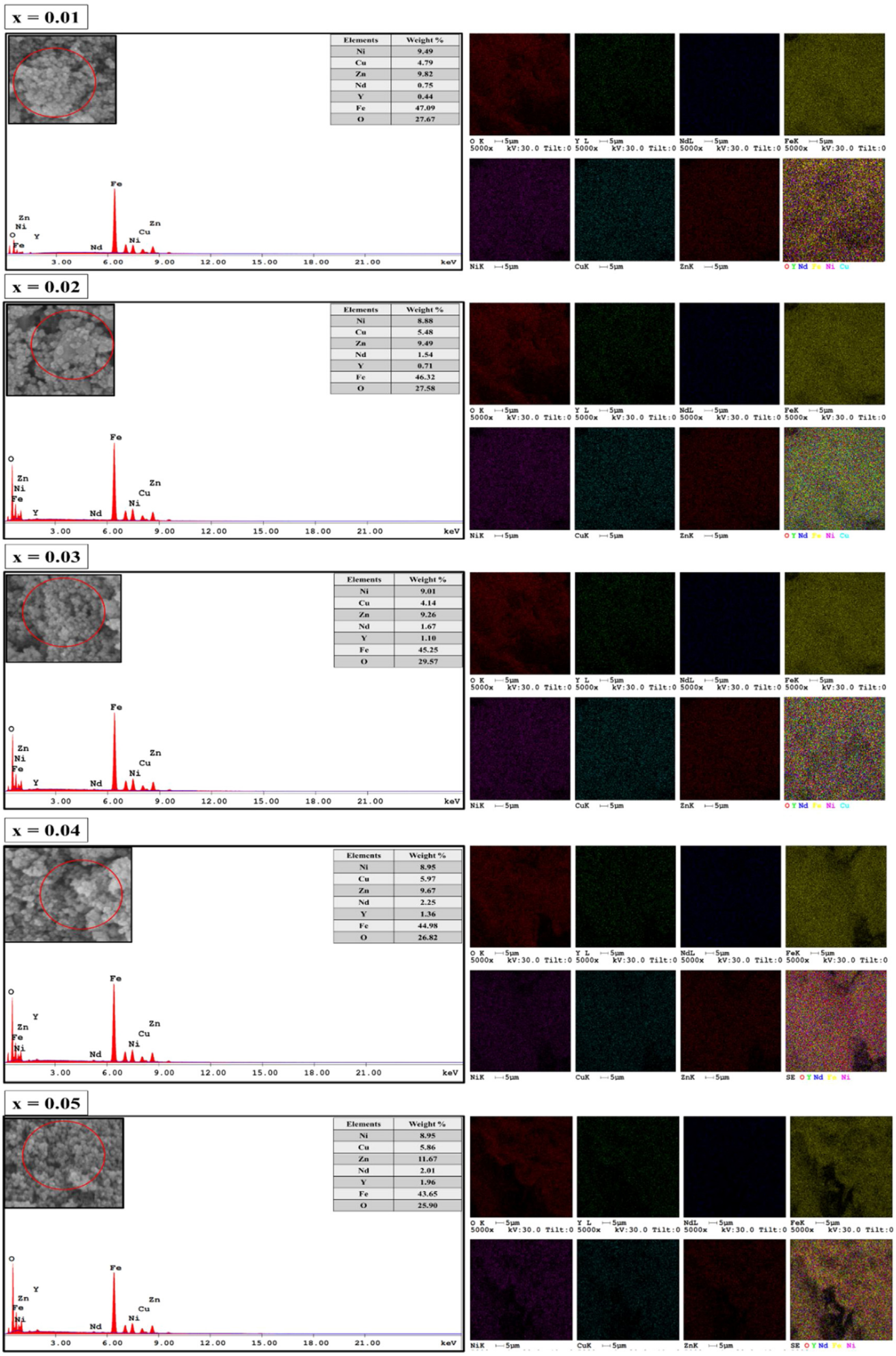

Fig. 3 – EDX spectra and elemental mapping of various prepared $[Ni_{0.4}Cu_{0.2}Zn_{0.4}](Nd_xY_xFe_{2-2x})O_4$ (x = 0.00-0.05) NSFs.

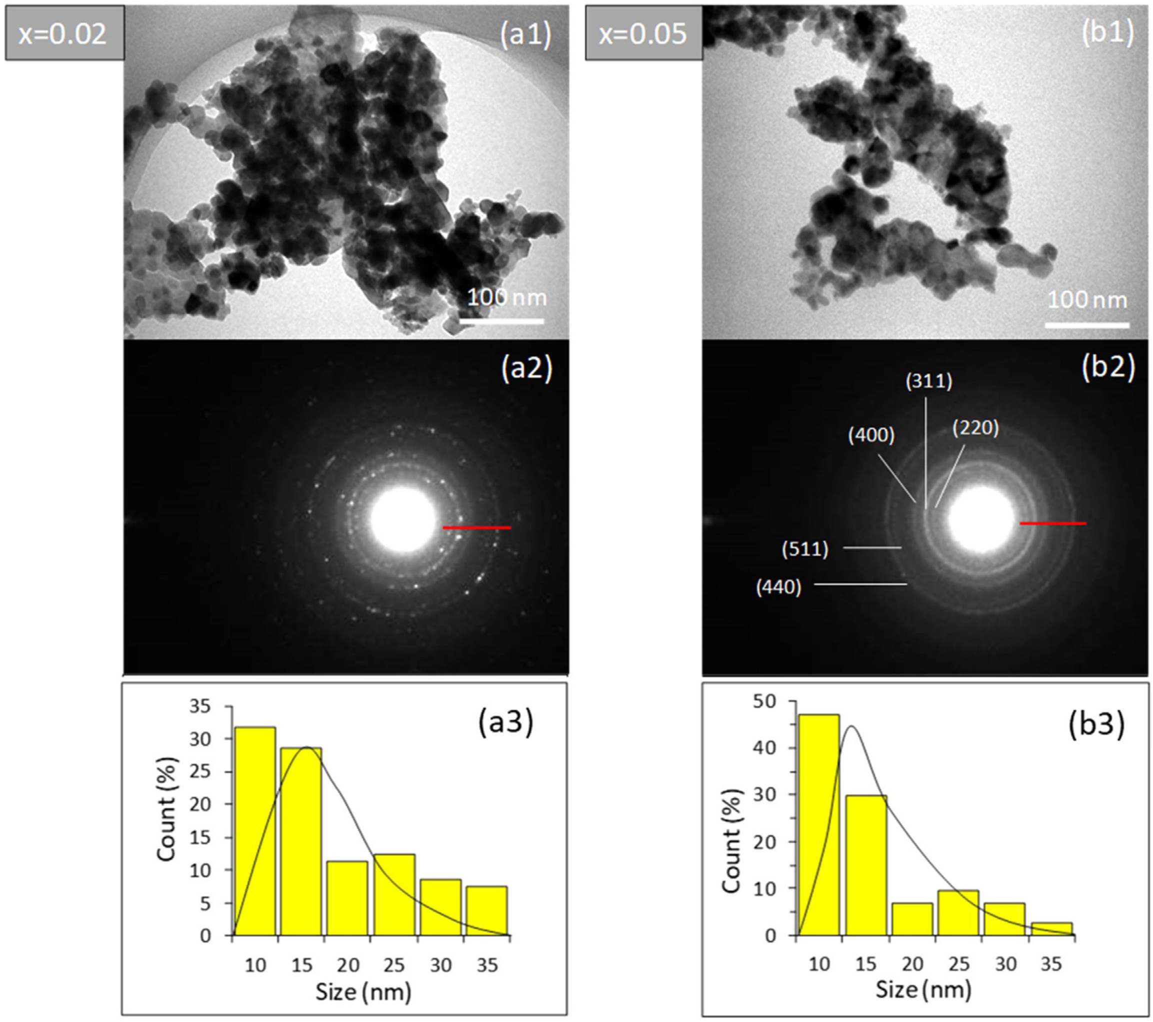

Fig. 4 – TEM images, SAED patterns, and particles size histograms of *[$Ni_{0.4}Cu_{0.2}Zn_{0.4}$]($Nd_xY_xFe_{2-2x}$)O_4* NSFs where x = 0.02 (a1–a3), and x = 0.05 (b1–b3).

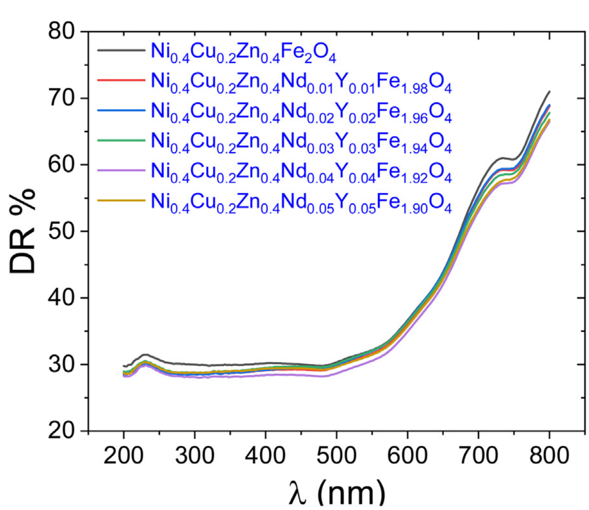

Fig. 5 – DR % *vs* λ spectra of *[$Ni_{0.4}Cu_{0.2}Zn_{0.4}$]($Nd_xY_xFe_{2-2x}$)O_4* (0.0 ≤ x ≤ 0.05) NSFs.

cates the recorded graphs with a sweep interval between 200 nm and 800 nm wavelength of electromagnetic spectrum. Energy of incident radiation corresponds to a range of 1.55 eV–6.2 eV for descending wavelength from 800 nm to 200 nm. DR % of all NiCuZn ferrite NSFs have magnitudes between 28.3–31.5% in range from 200 nm to 550 nm. Non-substituted $Ni_{0.4}Cu_{0.2}Zn_{0.4}Fe_2O_4$ mixed ferrite has an average reflectance of 30% in the same sweep range. Then DR % values belonging to all NPs increase almost directly (except a small plateau around 740 nm) and form a maximal band between 66–71% corresponding to wavelength of 800 nm in the rest sweep region. Scientific correlation to use DR % data to specify optical band gap (E_g) is based on Kubelka–Munk (*KM*) theory. *KM* function is directly proportional with absorption coefficient, α

$$KM = \frac{(1 - R_\infty)^2}{2R_\infty} = \alpha \quad (2)$$

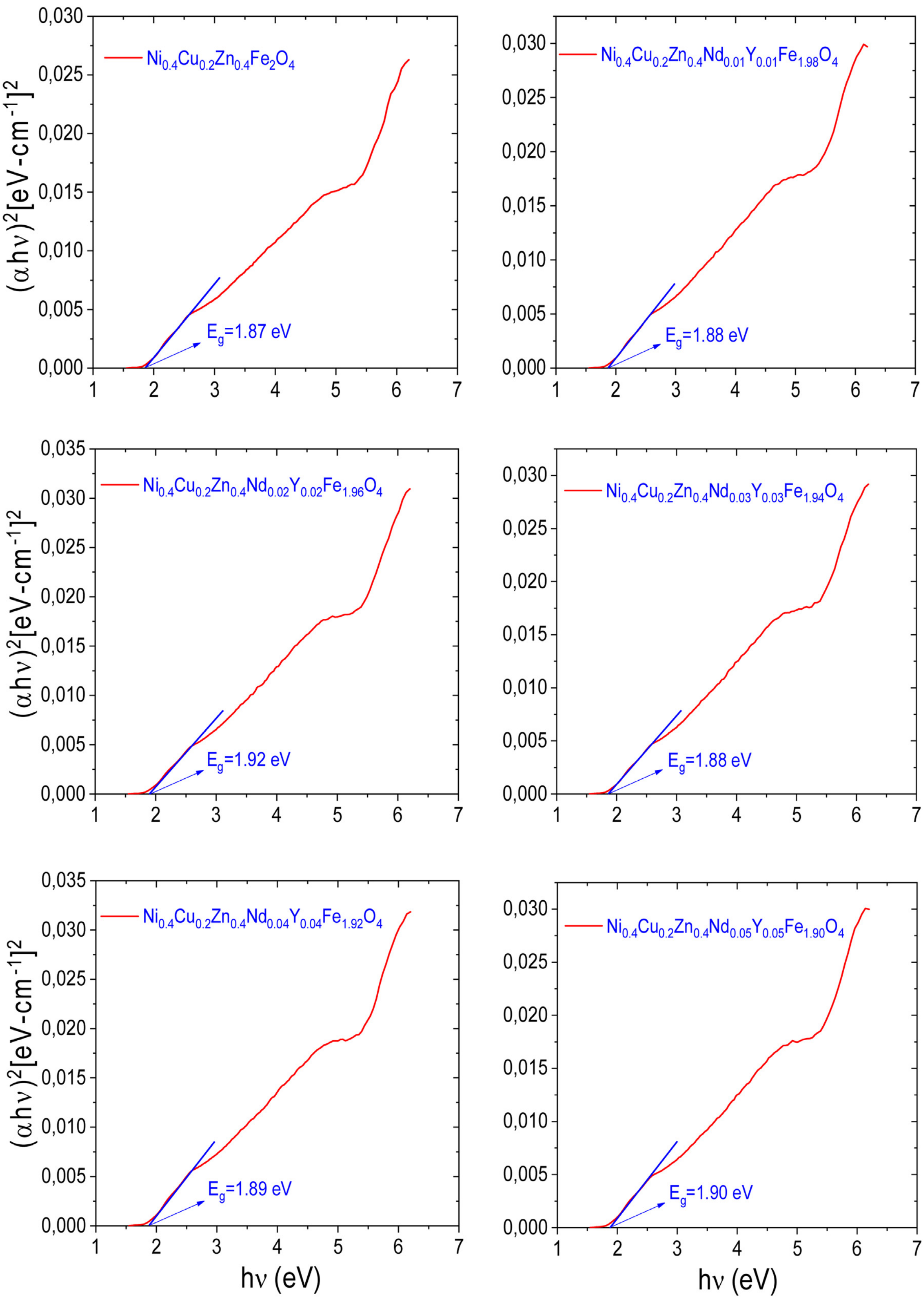

Fig. 6 – Tauc plots and extrapolated direct E_g data of $[Ni_{0.4}Cu_{0.2}Zn_{0.4}](Nd_xY_xFe_{2-2x})O_4$ ($0.0 \leq x \leq 0.05$) NSFs.

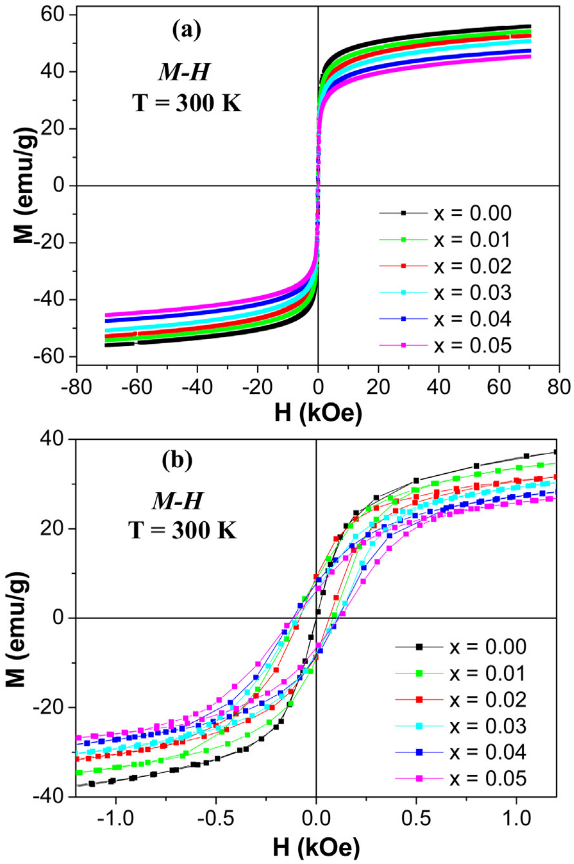

Fig. 7 – (M-H) curves of *$[Ni_{0.4}Cu_{0.2}Zn_{0.4}](Nd_xY_xFe_{2-2x})O_4$* ($0.0 \le x \le 0.05$) NSFs performed at room temperature.

Table 3 – RT magnetic parameters deduced from (M-H) measurements for $Ni_{0.4}Cu_{0.2}Zn_{0.4}](Nd_xY_xFe_{2-2x})O_4$ ($0.0 < x < 0.05$) NSFs.

x	M_s (emu/g)	M_r (emu/g)	H_c (Oe)	n_B (μ_B)
0.00	56.0	0.0	0.0	2.37
0.01	54.3	8.6	100.3	2.31
0.02	52.7	9.3	82.3	2.25
0.03	50.8	6.2	90.8	2.18
0.04	47.4	7.7	117.3	2.05
0.05	45.4	6.0	114.4	1.97

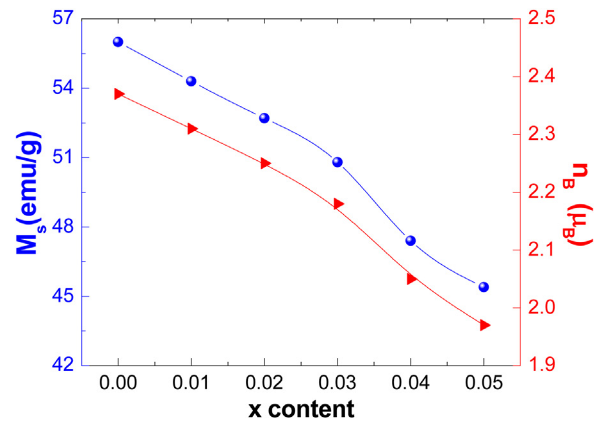

Fig. 8 – Variations in M_s and n_B values at RT with respect to Nd^{3+} and Y^{3+} contents for *$[Ni_{0.4}Cu_{0.2}Zn_{0.4}](Nd_xY_xFe_{2-2x})O_4$* ($0.0 \le x \le 0.05$) NSFs.

here, R_∞ is absolute remittance. E_g data are evaluated with Tauc and Davis–Mott model [21–24]:

$$(\alpha h\upsilon)^2 = A(h\upsilon - E_g) \tag{3}$$

here h is Planck's constant, υ is frequency of incident radiation and A is a constant of proportionality. Direct E_g values belonging to all $[Ni_{0.4}Cu_{0.2}Zn_{0.4}](Nd_xY_xFe_{2-2x})O_4$ ($x \le 0.05$) NSFs were obtained by extrapolating straight part of the Tauc plots. The graphs of $(\alpha h\upsilon)^2$ versus photon energy $h\upsilon$ to $(\alpha h\upsilon)^2 = 0$ are given in Fig. 6. Mixed but non-substituted $Ni_{0.4}Cu_{0.2}Zn_{0.4}Fe_2O_4$ NSFs has a band gap of 1.87 eV. Nd^{3+} and Y^{3+} ions substitutions where x = 0.01–0.05 caused slight increments. The direct E_g magnitudes were found between 1.88 and 1.92 eV. We could not reach any reported optical E_g data to compare our extrapolated results on Nd^{3+} and Y^{3+} ions substituted NiCuZn mixed ferrites in the literature. However, the E_g values of $Ni_{0.3}Cu_{0.3}Zn_{0.4}Tm_xFe_{2-x}O_4$ ($0.0 \le x \le 0.10$) FNPs manufactured by ultrasound irradiation technique was reported between 1.78 and 1.94 eV [25,26].

3.3. *Magnetic properties*

3.3.1. *Magnetization vs. magnetic field ((M-H))*

Fig. 7 illustrates RT magnetization (M) against magnetic field (H) for various prepared $[Ni_{0.4}Cu_{0.2}Zn_{0.4}](Nd_xY_xFe_{2-2x})O_4$ ($x \le 0.05$) NSFs. It is apparent that the non-substituted sample (x = 0.00) displayed superparamagnetic (SPM) character at RT with saturation magnetization M_s = 56.0 emu/g and no remanence (M_r) and coercivity (H_c). However, all substituted NPs soft ferrimagnetic (FM) behavior. Substituted NPs (x = 0.01–0.05) showed M_s values from 54.3 emu/g to 45.4 emu/g range, M_r values varying between 6.0 and 9.3 emu/g, and H_c magnitudes of 82.3–117.3 Oe. In high fields, we can apply the law of approach to saturation by linear fits of M vs. $1/H^2$ plots to obtain M_s values [27,28]. RT magnetic parameters are presented in Table 3 and Fig. 8.

The evolutions in M_s values and the experimental magnetic moments (n_B) are showed in Fig. 8. The n_B values were computed as follow [29,30]:

$$n_B = \frac{Moleculor\ weight \times M_s}{5585} \tag{4}$$

Non-substituted NiCuZn ferrite NSFs displayed M_s magnitude of about 56.0 emu/g at RT. These NPs prepared via ultrasonication route displayed larger M_s value than in those produced via SGAC [31,32] and in thin films of NiCuZn ferrites [33]. M_s do not show an increase trend with Nd^{3+} and Y^{3+} substitutions. It is perceived that M_s value diminished with increasing Nd^{3+} and Y^{3+} contents. The variation in crystallites size can affect in proportional way the magnetization amplitude [34,35]. In the present case, it is found that the D_{XRD} values decreased with rising Nd^{3+} and Y^{3+} contents, which is in line with M_s variations. Besides, the substitution of Fe^{3+} ions (0.64 Å) by larger ions Nd^{3+} (~0.98 Å) and Y^{3+} (~1.04 Å) produces structural disorder and strains within the ferrite system that affect greatly the electronic and magnetic properties [36]. Moreover, the decline in M_s could be accredited to the difference in magnetic moments of Fe^{3+}, Nd^{3+} and Y^{3+} ions [30]. Fe^{3+}, Nd^{3+} and Y^{3+} ions displayed magnetic moments of 5.0, 3.5, and 0.0 μ_B, respectively. So, it is assumed theoretically to view a reduction in magnetization value as a result of introducing lower magnetic moments of Nd^{3+} and Y^{3+} ions instead of some Fe^{3+} ions. In addition, the deduced values of n_B presented analogous trend of M_s variation regarding Nd^{3+} and Y^{3+} contents. RT M_s and n_B values are highest in non-substituted ferrite NPs and then reduced with increasing Nd^{3+} and Y^{3+} contents. The diminution in n_B is mainly resulted from the weakening in A–B super-exchange interactions [37].

3.3.2. *Magnetization against temperature (M-T)*

With the intention to further evaluate the influence of Nd-Y substitution on the NiCuZn NSFs, the magnetization was measured versus temperature from about 320 K down to around 2 K under ZFC–FC protocols at the field of 100 Oe. Fig. 9 showed the ZFC-FC magnetization curves for the selected x = 0.00, 0.01, 0.03 and 0.05 NPs. Both ZFC-FC magnetization magnitudes revealed a reduction with rising the Nd^{3+} and Y^{3+} substituting contents within Fe^{3+} sites. This is in conformity with (M-H) results. A change of a maximum in a ZFC plot is described as the blocking temperature (T_B). Above T_B, SPM characteristic is observed, while below T_B the SPM-FM transition occurred [38,39]. Figs. 9(a) and (b) belonging to non-substituted NiCuZn NSFs showed that the ZFC magnetization curve displays SPM

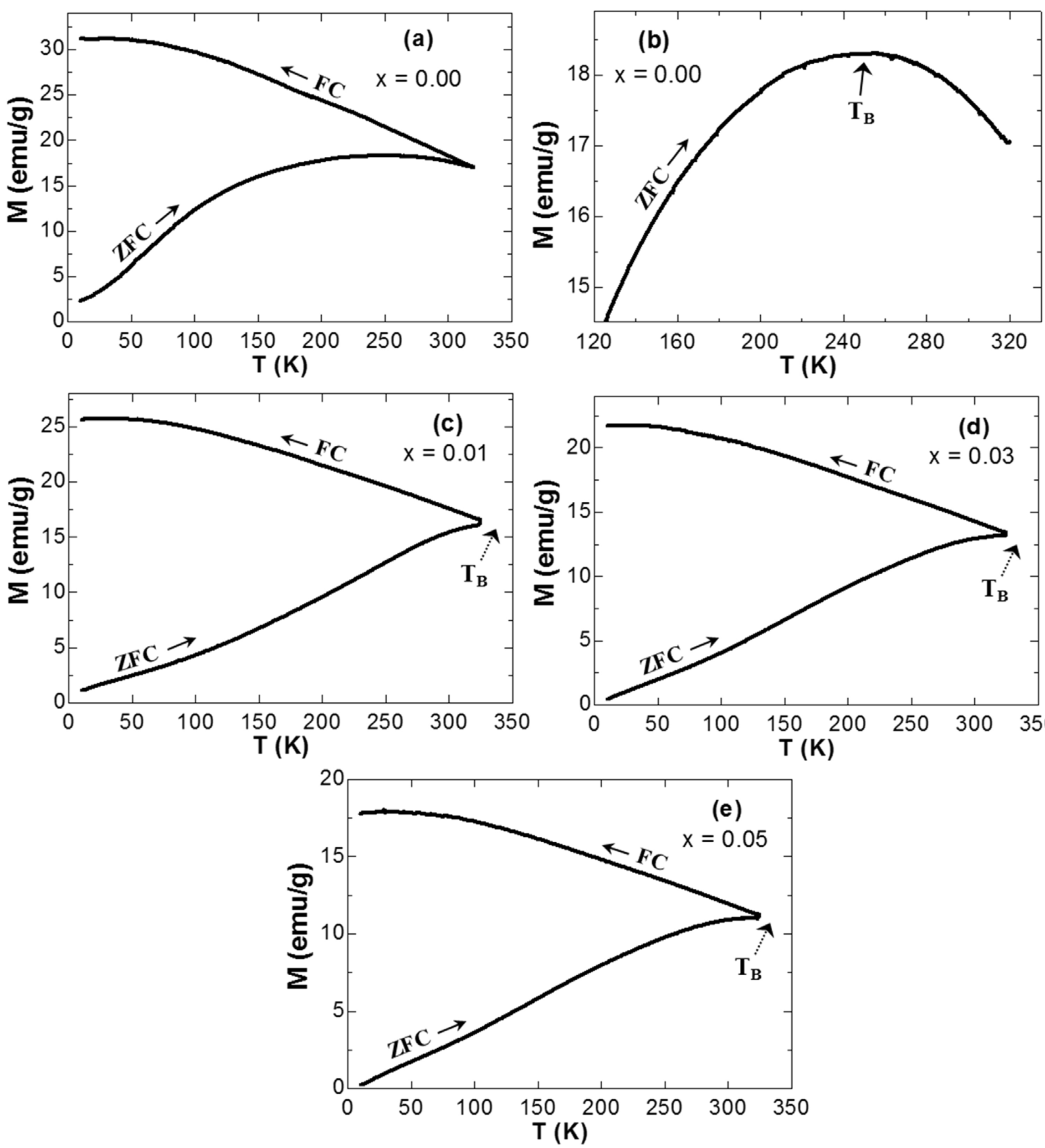

Fig. 9 – ZFC-FC magnetic measurements for *[Ni$_{0.4}$Cu$_{0.2}$Zn$_{0.4}$](Nd$_x$Y$_x$Fe$_{2-2x}$)O$_4$* (x = 0.00, 0.01, 0.03 and 0.05) NSFs.

relaxation within the experimental temperature interval. A broad peak around $T_B = 245$ K was observed in this product. However, Figs. 9(c–e) for various Nd-Y substituted NiCuZn ferrite NPs show that ZFC–FC magnetization plots do not exhibit SPM relaxation of the NPs throughout the temperature interval. The peak in ZFC curves of substituted samples lies down well overhead RT ($T_B > 320$ K) and no concrete superposition amongst FC and ZFC magnetization curves could be discerned. This implies a partially blocked state even at 320 K. Indeed, since FC-ZFC magnetization curves of Nd-Y substituted NiCuZn NSFs do not present any SPM relaxation up to 320 K, one can deduce that the coercive field is not null as the substituted NiCuZn NSFs are yet in a partially blocked state at 320 K. Our results are in line with the FM behavior observed in RT (M-H) hysteresis loops for various Nd-Y substituted NiCuZn FNPs.

A mutual characteristic of the various ZFC curves is the wide maximum area near T_B and the high T_B, which might denote large size distributions and large sizes, respectively. Nevertheless, the D_{XRD} values and SEM and TEM images showed small crystallites/grains/particles sizes, which are not sufficiently great to produce these high blocking temperatures. Another feature is that both ZFC-FC curves are bifurcated nearly to the observed extreme in ZFC curves at higher temperatures, representing thermal irreversibility in various products below 320 K. This implies feeble magnetic interactions between nanoparticles along with narrowed size of NPs in the products [40]. Furthermore, the large ZFC peak and the observed plateau or slow increase in FC magnetization curve at lower temperatures area designate moderate dipolar interactions [41]. Accordingly, the various above-declared characteristics of ZFC-FC magnetization curves can be resulted from the large inter-nanoparticles interactions (dipolar and surface-surface spin exchange and some nanoparticle agglomerations). Casula et al. [42] indicated that the small coercivities in Nd-Y substituted NiCuZn NSFs would be ascribed to NP dipolar interactions, which is also perceived in ZFC–FC magnetization curves. Accordingly, a total reduction of the magnetic characteristics of prepared MNPs is probably owing to the hindrance of the SPM relaxation by local frustrations in the mobility of magnetic moments provoked by the local distributions of fields [43]. The existence of dipolar interactions illuminates the partially blocked state detected in ZFC–FC magnetization curves and (M-H) loops at 300 K, and explains as well the overall reduction in magnetization.

3.4. *Microwave measurements*

According to the Maxwell's equations there are two main possible branches of electromagnetic absorption: due to electrical losses and due to magnetic losses. Electrical losses can be observed due to interaction of the electromagnetic radiation with charges in material (highly localized and conductive electrons; ions and dipoles). Electrical losses can be observed due to conductive losses; polarization losses; ionization losses; losses caused by heterogeneity of the structure. Magnetic losses can be associated with wave interactions with spin-orbital magnetic moments and domain states. There are two main types of magnetic losses: resonance of domain boundaries and natural ferromagnetic resonance (NFR).

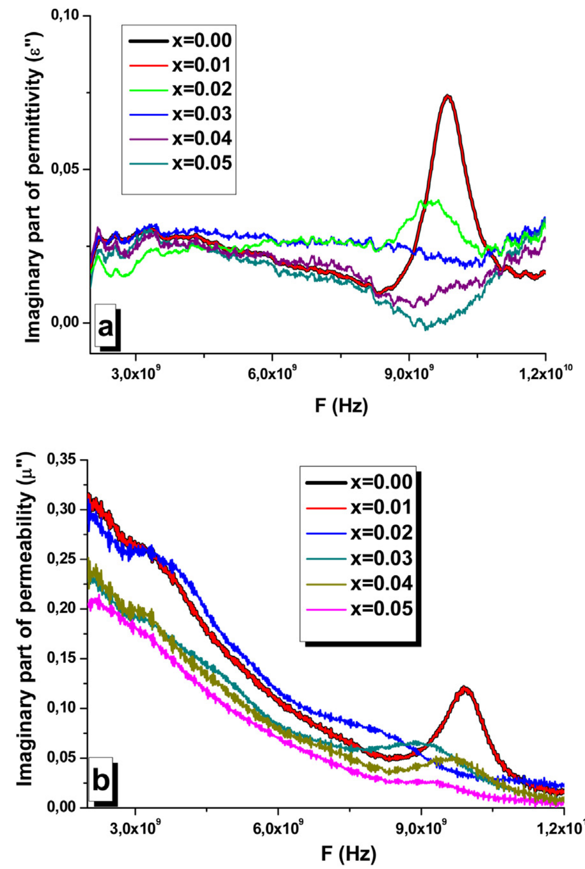

Fig. 10 – Frequency dependences of the imaginary parts of the electrical permittivity (a) and magnetic permeability (b) of x = 0.00, 0.01, 0.03 and 0.05.

Fig. 10 demonstrates frequency dependences of the microwave parameters: electrical permittivity (Fig.10a) and magnetic permeability (Fig.10b). It is interesting that for sample with low level of the chemical substitution ($x = 0.01$) there were no any changes in amplitude-frequency characteristics in comparison with the un-substituted $Ni_{0.4}Cu_{0.2}Zn_{0.4}Fe_2O_4$ NSFs. It was observed the maximum in the range 10−11 GHz on frequency dependences of the permittivity and permeability for $x = 0.00$ and 0.01 samples. It can be explained by the spin precession absorption of the electromagnetic radiation. Frequency of the spin precession for 3d-electrons of the Fe ions in ferrites determines the frequency of the absorbed energy [44,45]. The presence of the peaks on imaginary part of permittivity and permeability confirmed that the nature of the interaction between electromagnetic radiation and magnetic complex oxides is in NFR. The feature of the NFR in magnetic materials is due to the strong correlations between the spins of electrons that oscillating with the same frequency like external electromagnetic radiation. NFR attracts much attention due to possibility of the frequency-selective absorption (at resonant frequency the energy losses in the magnetic materials are maximal). The most interesting that “fingerprint” of the ferromagnetic resonance associated with non-linear increasing of the imaginary part of the magnetic permeability (presence of the peak on frequency dependence of the permeability). The data for $x = 0.00$ and 0.01 samples confirm

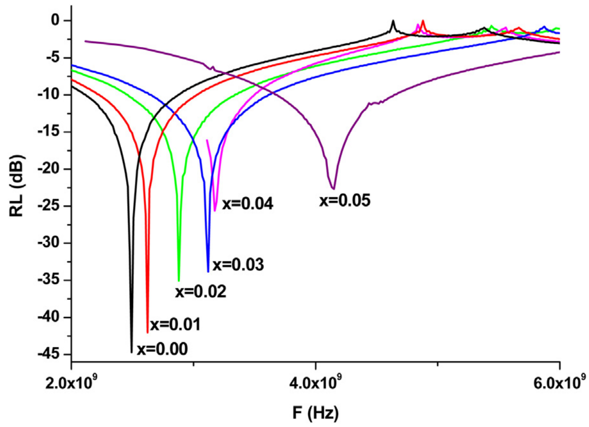

Fig. 11 – Frequency dependences of the RL of $[Ni_{0.4}Cu_{0.2}Zn_{0.4}](Nd_xY_xFe_{2-2x})O_4$ ($0.0 \le x \le 0.05$) NSFs.

that low level of substitution (less than 10 at.%) does not critically influence on energy system of system (frequency of the spin precession). Average values of the permittivity and permeability gradually reduced in comparison with the un-substituted $Ni_{0.4}Cu_{0.2}Zn_{0.4}Fe_2O_4$ NSFs. This due to decrease the Fe^{3+} ions number in spinel ferrite and weakening of the Fe—O—Fe exchange interaction by frustration of the magnetic structure [46].

For all investigated $[Ni_{0.4}Cu_{0.2}Zn_{0.4}](Nd_xY_xFe_{2-2x})O_4$ ($x \le 0.05$) NSFs, the most intense absorption of the electromagnetic radiation was observed at frequencies 2.49–4.15 GHz. On Fig. 11 presented frequency dependences of the RL (reflection coefficient) of the $[Ni_{0.4}Cu_{0.2}Zn_{0.4}](Nd_xY_xFe_{2-2x})O_4$ ($x \le 0.05$) NSFs. The global minimum of the RL named as amplitude of resonance (R_{Amp}) and the frequency which corresponds to the value R_{Amp} – frequency of resonance (R_{Freq}). The width of the peak is (width at ½ value of the R_{Amp}) band of resonance – R_{band}. The maximal value of absorption ($R_{Amp} = -44.69$ dB) was observed at 2.49 GHz (R_{Freq}) for un-substituted $Ni_{0.4}Cu_{0.2}Zn_{0.4}Fe_2O_4$ NSFs. Increase in the Nd^{3+}/Y^{3+} concentration from 0.00 to 0.05 led to an enhancement of R_{Freq} to 4.15 GHz and reduction of the R_{Amp} to −22.68 dB.

At the same time changing of the amplitude-frequency characteristics with increase of the Nd^{3+}/Y^{3+} concentration from x = 0.00 to x = 0.05 accompanied with the increase of the value R_{band} from 0.06 GHz to 0.55 GHz respectively. Fig. 12 demonstrates main amplitude-frequency characteristics: R_{amp}; R_{Freq}; R_{band}.

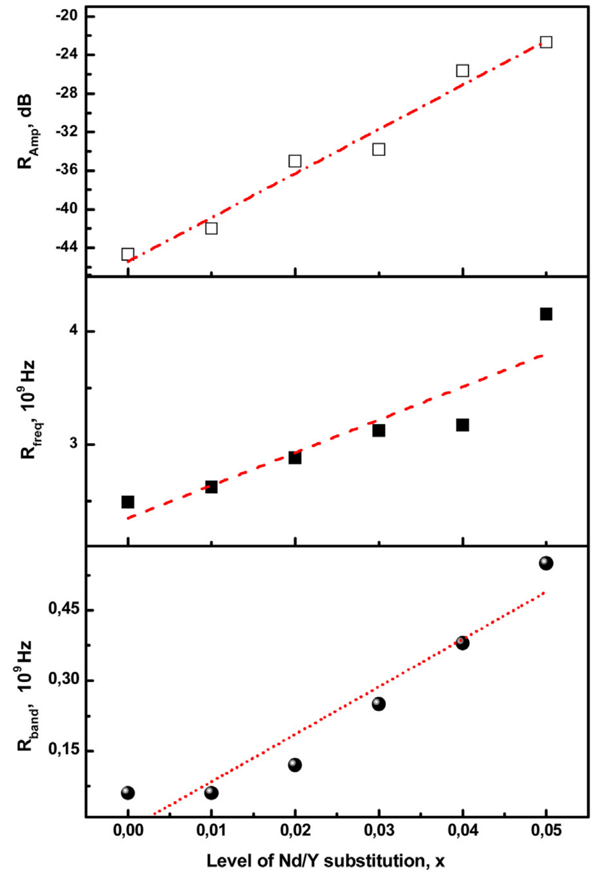

Fig. 12 – Frequency dependences of the main amplitude-frequency characteristics of $[Ni_{0.4}Cu_{0.2}Zn_{0.4}](Nd_xY_xFe_{2-2x})O_4$ ($0.0 \le x \le 0.05$) NSFs.

4. Conclusion

Spinel ferrites with nominal composition $[Ni_{0.4}Cu_{0.2}Zn_{0.4}](Nd_xY_xFe_{2-2x})O_4$ ($x \le 0.05$) NSFs were formed by the citrate sol-gel auto-combustion technique. The microstructure of compositions was approved through XRD, SEM, TEM and SAED. DRS % analyses proved direct and allowed electronic energy transitions for all non-ion and ion- substituted mixed ferrites. E_g values between 1.87 eV–1.92 eV validate the semiconducting nature of measured samples. Tuning ability of Nd^{3+} and Y^{3+} ions with x = 0.01–0.05 concentrations on band gap magnitudes are marginal. *(M-H)* curves at RT showed superparamagnetic (SPM) behavior in the non-substituted sample (x = 0.00). However, $[Ni_{0.4}Cu_{0.2}Zn_{0.4}](Nd_xY_xFe_{2-2x})O_4$ ($x \le 0.05$) NSFs exhibited soft ferrimagnetic (FM) character. It is found that the magnitude of magnetization decreases with increasing Nd^{3+} and Y^{3+} contents. This reduction is ascribed mainly to diminution in crystallite/particle size, deterioration of A–B super-exchange interactions, and variations in magnetic moments, etc. It is revealed an existence of dipolar interactions for various prepared samples, which illuminate the partially blocked state detected in ZFC–FC magnetization curves and M-H loops at 300 K, and explains as well the overall reduction in magnetization. The frequency dependences of the main electrodynamic parameters were investigated in the frequency range 2–12 GHz using co-axial line and calculated by the Nicholson-Ross-Weer method. The data for samples with low level of substitution (less than 10 at.%) confirmed that concentration of the Nd/Y x < 0.01 does not critically influence on energy system of system (frequency of the spin precession). For all investigated $[Ni_{0.4}Cu_{0.2}Zn_{0.4}](Nd_xY_xFe_{2-2x})O_4$ ($x \le 0.05$) NSFs, the most intense absorption of the electromagnetic radiation was observed at frequencies 2.49–4.15 GHz. The maximal value of absorption (−44.69 dB) was observed at 2.49 GHz for un-substituted $Ni_{0.4}Cu_{0.2}Zn_{0.4}Fe_2O_4$ NSFs. Increase in the Nd^{3+}/Y^{3+} concentration from 0.00 to 0.05 led to an enhancement of frequency of resonance to 4.15 GHz and reduction of the amplitude of resonance to −22.68 dB respectively. At the same time changing of the amplitude-frequency characteristics with increase of the Nd^{3+}/Y^{3+} concentration from x = 0.00 to x = 0.05 accompanied with the increase of the value R_{band} from 0.06 GHz to 0.55 GHz respectively. Almost linear behavior of the main AFC was observed. Results exposed possible applications of these types of materials in radio communication devices.

Declaration of interest statement

There are no conflicts of interest to declare.

Acknowledgments

The authors highly acknowledged the financial supports by the Institute for Research and Medical Consultations (Projects application No. 2018-IRMC-S-2) and by the Deanship for Scientific Research (Projects applications No. 2020-164-IRMC) of Imam Abdulrahman Bin Faisal University (Saudi Arabia). The work was partially supported by the Ministry of Science and Higher Education of the Russian Federation in the framework of Increase Competitiveness Program of NUST «MISiS» (grants No. P02-2017-2-4).

REFERENCES

[1] Shaterabadi Z, Nabiyouni G, Soleymani M. Physics responsible for heating efficiency and self-controlled temperature rise of magnetic nanoparticles in magnetic hyperthermia therapy. Prog Biophys Mol Bio 2018;133:9–19.
[2] Sanpo N, Berndt CC, Wen C, Wang J. Transition metal-substituted cobalt ferrite nanoparticles for biomedical applications. Acta Biomater 2013;9:5830–7.
[3] Batoo KM, Ansari MS. Low temperature-fired Ni-Cu-Zn ferrite nanoparticles through auto-combustion method for multilayer chip inductor applications. Nanoscale Res Lett 2012;7, 112-112.
[4] Kefeni KK, Msagati TA, Mamba BB. Ferrite nanoparticles: synthesis, characterisation and applications in electronic device. Mater Sci Eng B 2017;215:37–55.
[5] Li S, Meng Lin M, Toprak MS, Kim DK, Muhammed M. Nanocomposites of polymer and inorganic nanoparticles for optical and magnetic applications. Nano Rev 2010;1:5214.
[6] Pardavi-Horvath M. Microwave applications of soft ferrites. J Magn Magn Mater 2000;215-216:171–83.
[7] Paulsen J, Ring A, Lo C, Snyder J, Jiles DC. Manganese-substituted cobalt ferrite magnetostrictive materials for magnetic stress sensor applications. J Appl Phys 2005;97:044502.
[8] Luo J, Yue L, Ji H, Zhang K, Yu N. Investigation on the optimization, design and microwave absorption properties of $BaTb_{0.2}Eu_{0.2}Fe_{11.6}O_{19}$/PANI decorated on reduced graphene oxide nanocomposites. J Mater Sci 2019;54:6332–46.
[9] Hashim M, Shirsath SE, Meena SS, Kotnala RK, Kumar S, Ravinder D, et al. Superparamagnetic behavior of indium substituted NiCuZn nano ferrites. J Magn Magn Mater 2015;381:416–21.
[10] Aphesteguy JC, Damiani A, DiGiovanni D, Jacobo SE. Microwave-absorbing characteristics of epoxy resin composites containing nanoparticles of NiZn- and NiCuZn-ferrites. Physica B 2009;404:2713–6.
[11] Akhtar MN, Khan MA, Raza MR, Ahmad M, Murtaza G, Raza R, et al. Structural, morphological, dielectric and magnetic characterizations of Ni0.6Cu0.2Zn0.2Fe2O4 (NCZF/MWCNTs/PVDF) nanocomposites for multilayer chip inductor (MLCI) applications. Ceram Int 2014;40:15821–9.
[12] Slimani Y, Almessiere MA, Korkmaz AD, Guner S, Güngüneş H, Sertkol M, et al. Ni0.4Cu0.2Zn0.4TbxFe2-xO4 nanospinel ferrites: ultrasonic synthesis and physical properties. Ultrason Sonochem 2019;59:104757.
[13] Naik PP, Hasolkar SS, Kothawale MM, Keluskar SHP. Altering saturation magnetization of manganese zinc ferrite nanoparticles by doping with rare earth Nd^{+3} ions. Physica B 2020;584:412111.
[14] Qiana K, Yaoa Z, Lin H, Zhoua J, Haidry AA, Qia T, et al. The influence of Nd substitution in Ni–Zn ferrites for the improved microwave absorption properties. Ceram Int 2020;46:227–35.
[15] Jacobo SE, Bercoff PG. Structural and electromagnetic properties of yttrium-substituted Ni–Zn ferrites. Ceram Int 2016;42:7664–8.
[16] Chakrabarty S, Dutta A, Pal M. Effect of yttrium doping on structure, magnetic and electrical properties of nanocrystalline cobalt ferrite. J Magn Magn Mater 2018;461:69–75.
[17] Barathiraja C, Manikandan A, Mohideen AMU. Magnetically recyclable spinel $Mn_xNi_{1-x}Fe_2O_4$(x = 0.0–0.5) nano-photocatalysts: structural, morphological and opto-magnetic properties. J Supercond Nov Magn 2016;29:477–86.
[18] Shirsath SE, Mane ML, Yasukawa Y, Liu X, Morisako A. Chemical tuning of structure formation and combustion process in $CoDy_{0.1}Fe_{1.9}O_4$ nanoparticles: influence@pH. J Nanopart Res 2013;15:1976.
[19] Shirsath SE, Mane ML, Yasukawa Y, Liu X, Morisakoa A. Self-ignited high temperature synthesis and enhanced super-exchange interactions of Ho^{3+}–Mn^{2+}–Fe^{3+}–O^{2-} ferromagnetic nanoparticles. Phys Chem Chem Phys 2014;16:2347–57.
[20] Shirsath SE, Wang D, Jadhav SS, Mane ML, Li S. Ferrites obtained by sol-gel method. In: Klein L, Aparicio M, Jitianu A, editors. Handbook of sol-gel science and technology. Cham: Springer; 2018. p. 695–735.
[21] Auwal IA, Güner S, Güngüneş H, Baykal A. $Sr_{1-x}La_xFe_{12}O_{19}$ ($0.0 \le x \le 0.5$) hexaferrites: synthesis, characterizations, hyperfine interactions and magneto-optical properties. Cer Int 2016;42:12995–3003.
[22] Auwal IA, Güngüneş H, Güner S, Shirsath Sagar E, Sertkol M, Baykal A. Structural, magneto-optical properties and cation distribution of $SrBi_xLa_xY_xFe_{12-3x}O_{19}$ ($0.0 \le x \le 0.33$) hexaferrites. Mater Res Bull 2016;80:263–72.
[23] Baykal A, Guner S, Gungunes H, Batoo KM, Amir Md, Manikandan A. Magneto optical properties and hyperfine interactions of Cr^{3+} ion substituted copper ferrite nanoparticles. J Inorg Organomet Polym Mater 2018;28:2533–44.
[24] Tauc J, Grigorovici R, Vancu A. Optical properties and electronic structure of amorphous germanium. Phys Status Solidi 1966;15:627–37.
[25] Slimani Y, Almessiere MA, Sertkol M, Shirsath Sagar E, Baykal A, Nawaz M, et al. Structural, magnetic, optical properties and cation distribution of nanosized $Ni_{0.3}Cu_{0.3}Zn_{0.4}Tm_xFe_{2-x}O_4$ ($0.0 \le x \le 0.10$) spinel ferrites synthesized by ultrasound irradiation. Ultrason Sonochem 2019;57:203–11.

[26] George L, Viji C, Mathew H, Mohammed EM. Structural, dielectric, magnetic and optical properties of cerium substituted Ni-Zn mixed ferrite. Mater. Sci. Res. India 2017;14:133–9.

[27] Stoner EC, Wohlfarth E. A mechanism of magnetic hysteresis in heterogeneous alloys. Philosoph Trans R Soc London Series A Math Phys Sci 1948;240:599–642.

[28] Almessiere MA, Demir Korkmaz A, Slimani Y, Nawaz M, Ali S, Baykal A. Magneto-optical properties of rare earth metals substituted Co-Zn spinel nanoferrites. Ceram Int 2019;45:3449–58.

[29] Almessiere MA, Slimani Y, Kurtan U, Guner S, Sertkol M, Shirsath Sagar E, et al. Structural, magnetic, optical properties and cation distribution of nanosized $Co_{0.7}Zn_{0.3}Tm_xFe_{2\text{-}x}O_4$ ($0.0 \leq x \leq 0.04$) spinel ferrites synthesized by ultrasonic irradiation. Ultrason Sonochem 2019;58:104638.

[30] Almessiere MA, Slimani Y, Korkmaz AD, Taskhandi N, Sertkol M, Baykal A, et al. Sonochemical synthesis of Eu^{3+} substituted $CoFe_2O_4$ nanoparticles and their structural, optical and magnetic properties. Ultrason Sonochem 2019;58:104621.

[31] Chaudhari Vivek, Shirsath Sagar E, Mane ML, Kadam RH, Shelke SB, Mane DR. Crystallographic, magnetic and electrical properties of $Ni_{0.5}Cu_{0.25}Zn_{0.25}La_xFe_{2-x}O_4$ nanoparticles fabricated by sol–gel method. J Alloys Compd 2013;549:213–20.

[32] Roy PK, Bera J. Electromagnetic properties of samarium-substituted NiCuZn ferrite prepared by auto-combustion method. J Magn Magn Mater 2009;321:247–51.

[33] Liu Feng, Yang Chen, Ren Tianling, Wang AZ, Yu Jun, Liu Litian. NiCuZn ferrite thin films grown by a sol–gel method and rapid thermal annealing. J Magn Magn Mater 2007;309:75–9.

[34] Almessiere MA, Slimani Y, Güner S, Baykal A, Ercan I. Effect of dysprosium substitution on magnetic and structural properties of $NiFe_2O_4$nanoparticles. J Rare Earths 2019;37:871–8.

[35] Almessiere MA, Slimani Y, Güner S, Nawaz M, Baykal A, Aldakheel F, et al. Magnetic and structural characterization of Nb^{3+}-substituted $CoFe_2O_4$ nanoparticles. Ceram Int 2019;45:8222–32.

[36] Slimani Y, Güngüneş H, Nawaz M, Manikandan A, El Sayed H, Almessiere M, et al. Magneto-optical and microstructural properties of spinel cubic copper ferrites with Li-Al co-substitution. Ceram Int 2018;44:14242–50.

[37] Slimani Y, Almessiere MA, Nawaz M, Baykal A, Akhtar S, Ercan I, et al. Effect of bimetallic (Ca, Mg) substitution on magneto-optical properties of $NiFe_2O_4$ nanoparticles. Ceram Int 2019;45:6021–9.

[38] Slimani Y, Unal B, Almessiere MA, Demir Korkmaz A, Shirsath Sagar E, Yasin Ghulam, et al. Investigation of structural and physical properties of Eu3+ ions substituted $Ni_{0.4}Cu_{0.2}Zn_{0.4}Fe_2O_4$ spinel ferrite nanoparticles prepared via sonochemical approach. Results Phys 2020;17:103061.

[39] Humbe AV, Kounsalye JS, Shisode MV, Jadhav KM. Rietveld refinement, morphology and superparamagnetism of nanocrystalline $Ni_{0.70-x}Cu_xZn_{0.30}Fe_2O_4$ spinel ferrite. Ceram Int 2018;44:5466–72.

[40] Predoi D, Kuncser V, Tronc E, Nogues M, Russo U, Principi G, et al. Magnetic relaxation phenomena and inter-particle interactions in nanosized γ-Fe_2O_3 systems. J Phys Condens Matter 2003;15:1797.

[41] Kostopoulou A, Brintakis K, Vasilakaki M, Trohidou KN, Douvalis AP, Lascialfari A, et al. Assembly-mediated interplay of dipolar interactions and surface spin disorder in colloidal maghemite nanoclusters. Nanoscale 2014;6:3764–76.

[42] Casula MF, Conca E, Bakaimi I, Sathya A, Materia ME, Casu A, et al. Manganese doped-iron oxide nanoparticle clusters and their potential as agents for magnetic resonance imaging and hyperthermia. Phys Chem Chem Phys 2016;18:16848–55.

[43] Dutz S, Clement JH, Eberbeck D, Gelbrich T, Hergt R, Muller R, et al. Ferrofluids of magnetic multicore nanoparticles for biomedical applications. J Magn Magn Mater 2009;321:1501–4.

[44] Almessiere MA, Trukhanov AV, Khan FA, Slimani Y, Tashkandi N, Turchenko VA, et al. Correlation between microstructure parameters and anti-cancer activity of the $[Mn_{0.5}Zn_{0.5}](Eu_xNd_xFe_{2\text{-}2x})O_4$ nanoferrites produced by modified sol-gel and ultrasonic methods. Ceram Int 2020;46:7346–54.

[45] Almessiere MA, Slimani Y, Güngüneş H, Kostishyn VG, Trukhanov SV, Trukhanov AV, et al. Impact of Eu^{3+} ions substitution on structural, magnetic and microwave traits of Ni-Cu-Zn spinel ferrites. Ceram Int 2020;46:11124–31.

[46] Trukhanov AV, Kostishyn VG, Panina LV, Korovushkin VV, Turchenko VA, Thakur P, et al. Control of electromagnetic properties in substituted electromagnetic properties in substituted M-type hexagonal ferrites. J Alloys Compd 2018;754:247–56.

Update

Journal of Materials Research and Technology
Volume 32, Issue , September - October 2024, Page 4122–4123

DOI: https://doi.org/10.1016/j.jmrt.2024.08.200

Journal of Materials Research and Technology 32 (2024) 4122–4123

Contents lists available at ScienceDirect

Journal of Materials Research and Technology

journal homepage: www.elsevier.com/locate/jmrt

Corrigendum to “Effect of Nd–Y co-substitution on structural, magnetic, ptical and microwave properties of NiCuZn nanospinel ferrites” [J Mater Res Technol, Volume **9**, Issue 5, September–October 2020, Pages 1278-11290]

.A. Almessiere [a,**], Y. Slimani [a,*], A.V. Trukhanov [b,c,d], A. Demir Korkmaz [e], S. Guner [f], . Akhtar [a], Sagar E. Shirsath [g], A. Baykal [h], I. Ercan [a]

Department of Biophysics, Institute for Research and Medical Consultations (IRMC), Imam Abdulrahman Bin Faisal University, P.O. Box 1982, Dammam, 31441, audi Arabia
SSPA “Scientific and Practical Materials Research Centre of NAS of Belarus”, 19, P. Brovki Str., 220072, Minsk, Belarus
South Ural State University, 76, Lenina Ave., 454080, Chelyabinsk, Russia
National University of Science and Technology MISiS, Moscow, 4, Leninsky Prospekt, 119049, Russia
Department of Chemistry, Istanbul Medeniyet University, 34700, Uskudar, Istanbul, Turkey
Institute of Inorganic Chemistry, RWTH Aachen University, D-52074, Aachen, Germany
School of Materials Science and Engineering, University of New South Wales, Kensington, Sydney, NSW, 2052, Australia
Department of Nanomedicine Research, Institute for Research and Medical Consultations (IRMC), Imam Abdulrahman Bin Faisal University, P.O. Box 1982, Dammam, 1441, Saudi Arabia

The authors regret to inform that there is an error in Fig. 2 in the riginal published version of the article (https://doi.org/10.1016/j.jmrt 2020.08.027) as some SEM images were unintentionally duplicated uring the process of copying and pasting from multiple SEM files, the rrangement of different images into the PowerPoint, and then the seection of images to be presented in the paper. Fortunately, the authors confirm that no any of the other results were affected by this unintentional error.

The corrected version of Fig. 2 is attached.

The authors would like to apologise for any inconvenience caused by this unintentional error.

DOI of original article: https://doi.org/10.1016/j.jmrt.2020.08.027.

* Corresponding author.
** Corresponding author.
E-mail addresses: malmessiere@iau.edu.sa (M.A. Almessiere), yaslimani@iau.edu.sa (Y. Slimani).

ttps://doi.org/10.1016/j.jmrt.2024.08.200

vailable online 1 September 2024

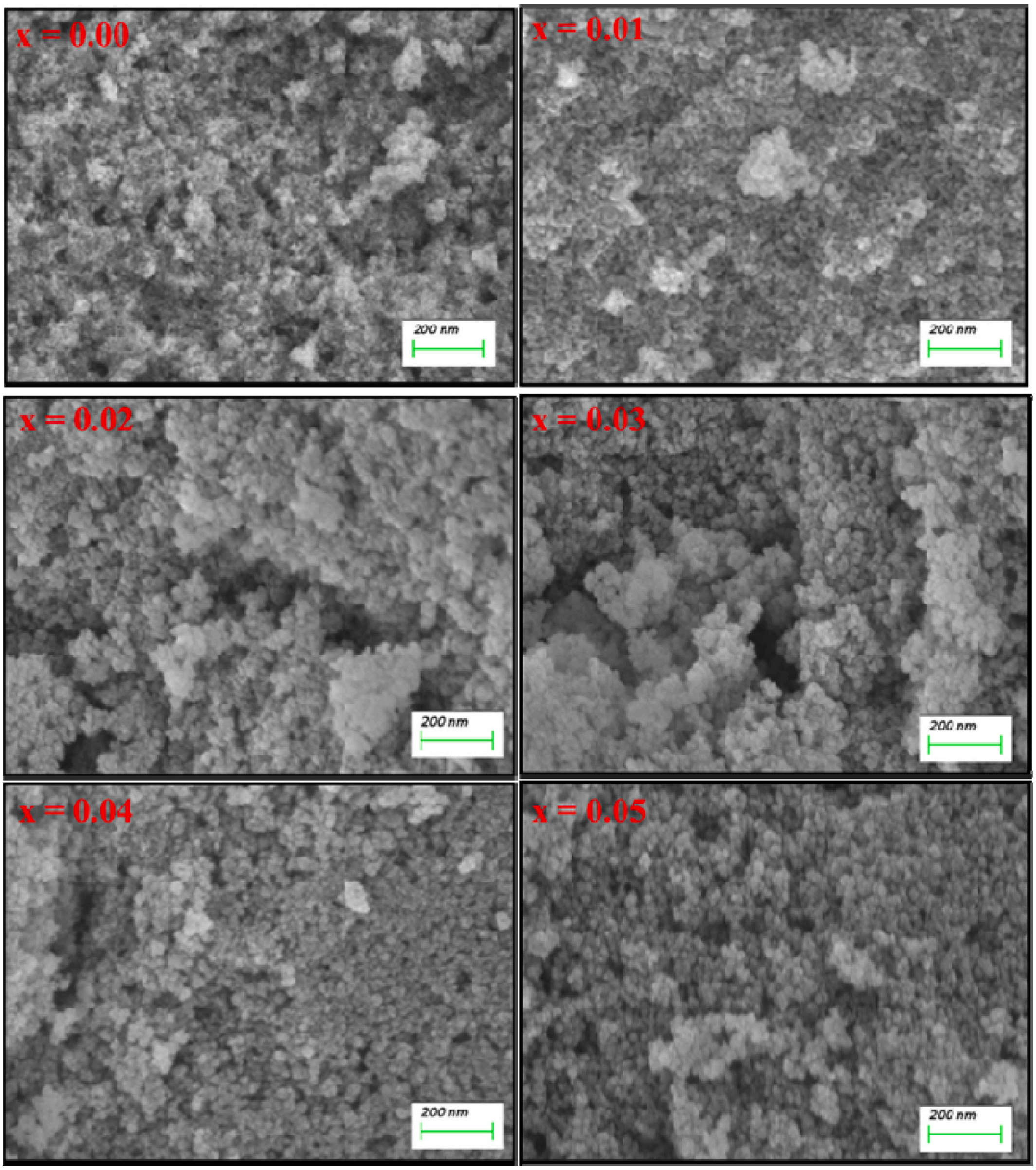

Fig. 2. SEM images of $[Ni_{0.4}Cu_{0.2}Zn_{0.4}](Nd_xY_xFe_{2\text{-}2x})O_4$ ($0.0 \leq x \leq 0.05$) NSFs.